Experimental Investigation of Momentum Transfer to Solid Surfaces by the Impact of Energetic Ions and Atoms

IEPC-2013-329

Presented at the 33rd International Electric Propulsion Conference,
The George Washington University, Washington, D.C., USA
October 6–10, 2013

Thomas Trottenberg*, Jakob Rutscher†, and Holger Kersten‡
Institute of Experimental and Applied Physics, University of Kiel, 24098 Kiel, Germany

Abstract: This paper presents an instrument for the direct experimental determination of (one component of) the momentum that is transferred to a target at the interaction with energetic atoms or ions. Special attention is paid to the case of kinetic energies above the sputtering threshold. The importance of momentum transfer at gas–surface interactions for space applications is highlighted, and a direct measurement of atmospheric drag coefficients by means of a force probe is suggested.

Nomenclature

A_{eff}	= effective cross-section of an object in orbit
α, α_{up}, α_{down}	= angular acceleration, acceleration at speeding up and slowing down
c_{d}	= drag coefficient of an object in orbit
$c_{\parallel}$, $c_{\perp}$	= momentum transfer coefficients parallel and perpendicular to the beam
E, $\dot{E}$	= total energy of an object in orbit, energy loss rate due to drag
ΔE	= energy difference for neighboring orbits
E_{kin}, E_{pot}	= kinetic and potential energies of an object in orbit
F_{beam}	= force exerted onto a target by a beam
F_{d}	= drag force of an object in orbit
$\Gamma_{\mathrm{i}}(z)$, $\Gamma_{\mathrm{i+n}}(z)$	= ion and total flux densities at distance z from the beam source
I	= moment of inertia
λ_{cx}	= mean free path for charge-exchange collisions
M	= accelerating torque
M_{beam}, M_{fr}	= accelerating torques caused by the beam and friction
$\vec{p}_{\mathrm{in}}$, $\vec{p}_{\mathrm{out}}$	= momenta of the impinging and the outgoing particles
$\vec{p}_{\parallel}$, $\vec{p}_{\perp}$	= momenta of the outgoing particles parallel and perpendicular to the beam
r	= distance of the target centers from the rotational axis
ρ_{gas}, ρ_{p}	= mass densities of the rarefied atmosphere and an object in orbit
t, Δt	= time, time step
v, v_{esc}	= velocity of an object in orbit, escape velocity
z	= distance z from the beam source

*Research Associate, Plasma Technology, trottenberg@physik.uni-kiel.de
†Former student, Plasma Technology, rutscher@physik.uni-kiel.de
‡Professor, Plasma Technology, kersten@physik.uni-kiel.de

I. Introduction

Interaction of energetic atoms and ions with matter, especially sputtering, is an important phenomenon for many space applications. Sputtering causes, as a disadvantageous side effect, grid erosion in ion thrusters and determines the life expectancy of the engines.[1,2] Hall thrusters are affected by ceramic erosion.[3] Sputter erosion might also be important in helicon plasma thrusters like VASIMR.[4] Solar panels suffer from unintentional bombardment with plume ions, because sputtering downgrades the optical transmission of the cover glass.[5] Furthermore, optical devices can be contaminated indirectly by deposition of the sputtered material. Also natural sources of energetic atoms and ions interact with surfaces of space vehicles, for example satellites and small objects in low Earth orbits. However, the kinetic energies of the air molecules with respect to the object in the orbit remain below the sputter thresholds. Therefore, the kind of reflection of the air molecules determines the momentum transfer to the orbiter and the so-called drag coefficient. In case of a satellite, e.g. the at a height of 270 km operating GOCE, this momentum transfer equals the thrust needed to counteract the air drag. In case of objects without propulsion, e.g. space debris of different sizes, the drag force is crucial for the orbital life time, i.e. length of time the object remains in orbit.

Recently, several beneficial applications of beam–surface interaction in space were proposed. One of them is the "ion beam shepherd" concept for space debris removal. A collimated ion beam is to be produced on a spacecraft flying close to the debris object and directed onto the object in order to modify its orbit.[6] As another application, the "ion beam sail" propulsion concept was discussed, where the ion source is not onboard the propelled space vehicle, but on a space station or the moon, and the beam pushes an electrostatic sail produced by the vehicle that is to be propelled.[7] Authors from the Ad Astra Rocket Company propose a system of two in opposed directions thrusting VASIMR engines that allows to move a near-Earth asteroid to a high lunar orbit or to deflect a "dangerous" asteroid that could otherwise impact on Earth.[8]

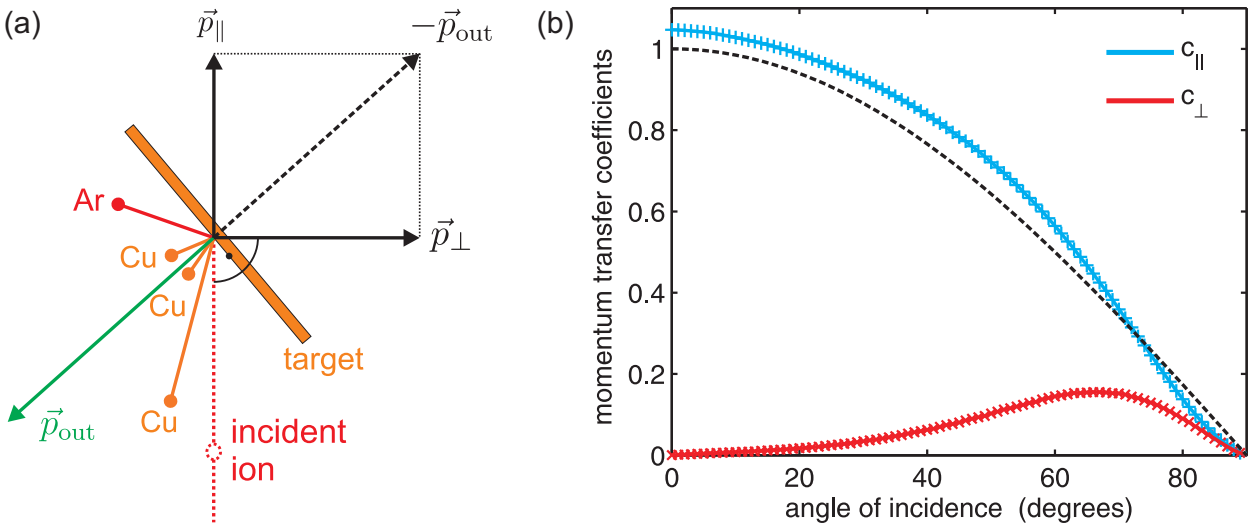

Figure 1. (a) Example of a single sputter event and momenta related to the outgoing particles. (b) Parallel and perpendicular momentum transfer coefficients (SRIM simulation for 1200 eV argon ions impinging on glass). The dashed line is a cosine function and corresponds to a perfectly absorbing surface without sputtering.

In this work, we investigate experimentally the physics behind these phenomena and applications, i.e. the momentum transfer from energetic ions and atoms to solid targets. Figure 1(a) illustrates an ion impact event of an argon ion, which produces three sputtered copper atoms. The argon ion itself is inelastically reflected. In this situation, not only the momentum $\vec{p}_{\mathrm{in}}$ of the incident ion is transferred to the surface: The vector $\vec{p}_{\mathrm{out}}$ is the sum of the momenta of the four outgoing particles, and due to conservation of momentum, $-\vec{p}_{\mathrm{out}}$ is transferred to the target, too. The total transferred momentum is therefore the vector $\vec{p}_{\mathrm{in}} - \vec{p}_{\mathrm{out}}$, which in general is oblique to the direction of the beam.

In many situations, $\vec{p}_{\mathrm{in}} + \vec{p}_{\parallel}$, i.e. the component parallel to the direction of the incident particles, is of primary importance, for example, in the above mentioned proposed concepts. If the perpendicular components $\vec{p}_{\perp}$ of all the surface elements do not cancel out, then the tugged object would experience an oblique acceleration. The force exerted along the direction of the beam can be measured directly by force

probes.[9–11] The force perpendicular to the direction of the beam can also be measured.[12,13] In this paper, we describe a device for the measurement of this perpendicular component and compare our measurements with sputter simulations. Figure 1(b) shows a typical simulation of the two components for different angles of incidence. Instead of the absolute momenta, the scalar momentum transfer coefficients $c_{\parallel} = |\vec{p}_{\mathrm{in}} + \vec{p}_{\parallel}|/|\vec{p}_{\mathrm{in}}|$ and $c_{\perp} = |\vec{p}_{\perp}|/|\vec{p}_{\mathrm{in}}|$, i.e. the parallel and perpendicular components of the transferred momenta normalized to the momentum of an incident particle $|\vec{p}_{\mathrm{in}}|$, are shown.

An interesting application is the above mentioned prediction of the orbital life time of small objects in a low Earth orbit (LEO). We calculate trajectories for spherical model objects based on the empirical NRLMSIS-00 model of the Earth's atmosphere[14] and an assumption of the momentum transfer from the atmospheric gas molecules impacting on the objects.

II. The sputter-propelled instrument

For the measurement of the momentum carried by the released particles in a sputter process, we designed the "sputter-propelled instrument" (SPIN) that uses this momentum to set a movable target in motion. The sputter-propelled instrument has a rotor similar to a cross-shaped windmill rotor, however, in this case, the rotor is oriented horizontally and the ion beam is directed vertically upwards.

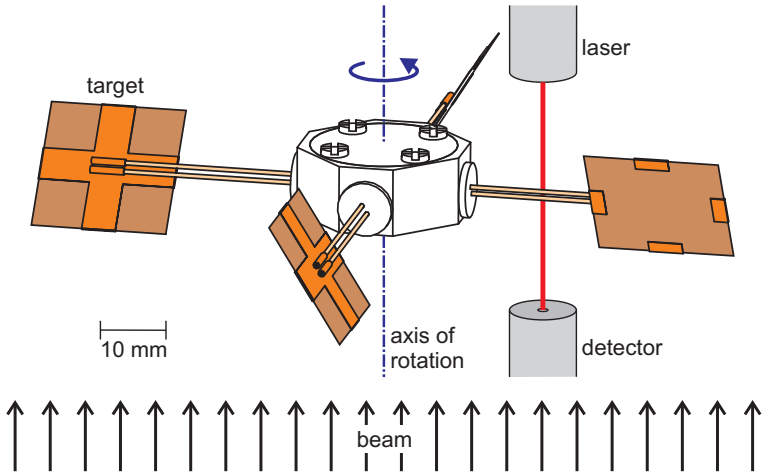

Figure 2. Drawing of the sputter-propelled instrument (SPIN). The supporting needle on the axis is not shown.

Figure 2 shows the setup with the only 10 g light rotor with a diameter of about 10 cm. Four thin square target plates, each one with an area of $20 \times 20\,\mathrm{mm}^2$, are mounted like the blades of a cross-shaped windmill rotor. The rotor blades can be tilted in order to adjust the angle of incidence of the beam particles. The rotor is supported with a bearing with conical cavity resting on a needle tip above its center of mass, which ensures a stable horizontal equilibrium. A photodiode detects the transits of the ceramic rotor arms through a light beam for a calculation of the angular acceleration α. The targets are electrically connected by wires through the ceramic tubes and from there via the bearing and the needle to an external voltage source. This allows biasing and a measurement of the target current. The targets were biased negatively with $-20\,\mathrm{V}$ in the experiments.

The momentum transfer from a particle beam to a target surface can be devided in incoming and outgoing parts: the first one is the momentum of the incident particles, and the second one is the momentum of all the particles which leave the target, i.e. sputtered target atoms and, much less frequent, "reflected" beam particles. In case of the force probes which measure the force component in the direction of the incident particles, the sum of the momenta of the incoming and outgoing particles is measured.[9–11] In contrast, the here presented SPIN can react only in a direction perpendicular to the beam, hence, it is sensitive only to the momentum of sputtered target atoms and reflected beam particles, but insensitive to the momentum of the impinging particles [see Fig. 1(a)]. Only the momentum of the outgoing particles may have a component in the direction of the degree of freedom.

For a calculation of the accelerating torque $M = I\alpha$, the moment of inertia I was determined in a pre-

liminary torsion pendulum experiment, where the rotor was hanging on a torsion wire. The net accelerating torque

$$M = M_{\mathrm{beam}} - M_{\mathrm{fr}} \tag{1}$$

is the torsional moment caused by the force acting on the four targets M_{beam} lowered by some friction M_{fr}. Assuming kinetic friction in the bearing, M_{fr} is independent of the sliding velocity and even of the perhaps variable area of friction. In order to determine the constant friction M_{fr}, each measurement of the angular acceleration $\alpha = \alpha_{\mathrm{up}} > 0$ with the beam switched on is supplemented by a measurement of the running down process, i.e. the angular acceleration $\alpha = \alpha_{\mathrm{down}} < 0$ is measured when the beam is switched off [see Fig. 3(a)]. In the latter case is $M_{\mathrm{fr}} = I\alpha_{\mathrm{down}}$, which enables a calculation of M_{beam}.

The force on the area of the four targets becomes $F_{\mathrm{beam}} = M_{\mathrm{beam}}/r$, or

$$F_{\mathrm{beam}} = \frac{I}{r}(\alpha_{\mathrm{up}} - \alpha_{\mathrm{down}}) \quad , \tag{2}$$

where $r = 41\,\mathrm{mm}$ is the distance of the target centers to the rotational axis.

III. Results from measurements and simulations

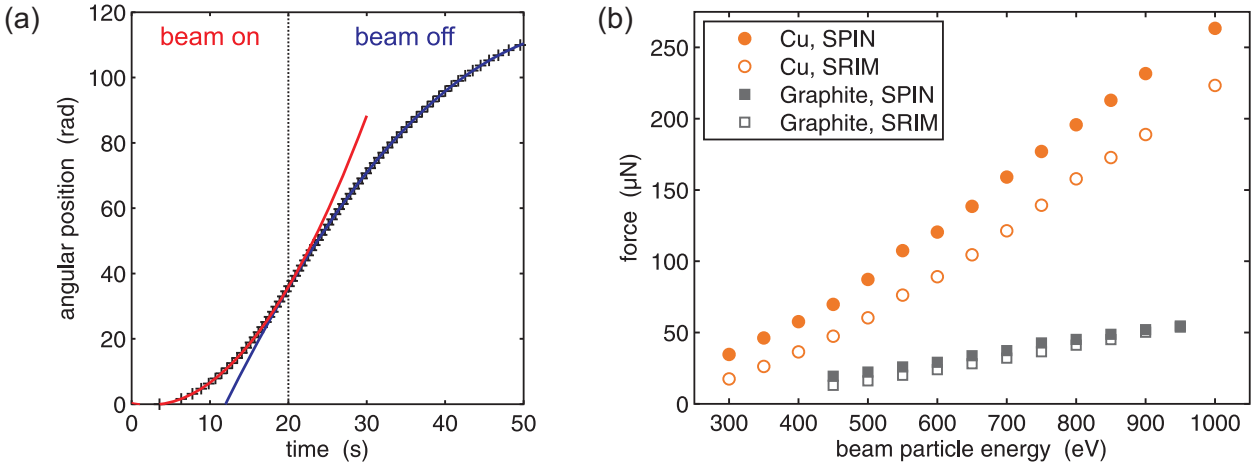

Figure 3. (a) Acceleration and running down processes together with parabolic fits. (b) Measured repulsive forces due to sputtered atoms and recoil beam particles for two target materials.[13]

In Fig. 3(b), measurements for two different target materials are shown. The beam parameters, in particular the distance of the targets from the grids of $19,2\,\mathrm{cm}$, the angle of incidence of $56°$, and the gas pressure of $2 \times 10^{-2}\,\mathrm{Pa}$, are the same in both cases. The copper target yields a significantly higher accelerating force than the graphite target.

Simulations of the argon impact events are carried out with the SRIM Monte Carlo code for calculations of the interaction of energetic ions with amorphous targets.[15,16] The code provides energies and directions of the sputtered atoms and the recoil ions. Summation of the individual momenta[17] and projection onto the horizontal rotor plane allows a comparison with the measured data. The impact rate is obtained from the current measurement and inclusion of the neutral component according to

$$\Gamma_{\mathrm{i}}(z) = \Gamma_{\mathrm{i+n}}(z) \exp\left(-\frac{z}{\lambda_{\mathrm{cx}}}\right) \quad . \tag{3}$$

This equation describes, that the ion flux density $\Gamma_{\mathrm{i}}(z)$ as a function of the distance z from the ion source is determined by two factors: the first one, $\Gamma_{\mathrm{i+n}}(z)$, is the total flux of beam particles regardless of their charge, i.e. ions and neutral atoms together, and decays due to the geometrical beam expansion. The second one, $\exp(-z/\lambda_{\mathrm{cx}})$, is the neutralization of the beam due to charge-exchange collisions, where λ_{cx} is the mean free path for charge-exchange collisions. Charge-exchange collisions are the dominating process for kinetic energies above $100\,\mathrm{eV}$.[18] An important feature of charge-exchange collisions is that the original ion loses its charge, but practically maintains its energy and direction.[19] From the point of view of the sputter process,

the charge state of the impinging atom is of minor importance,[15] so that the total beam flux density $\Gamma_{\mathrm{i+n}}(z)$ rather than the ion beam flux density determines the rate at which sputter cascades are initiated.

The sputter-propelled instrument is a straightforward method for an experimental determination of (one component of) the momentum transferred by a beam of ions and neutral atoms to a surface. The targets can be replaced by targets of other materials and the angle of incidence can be varied.

However, SPIN measures only the component perpendicular to the incident beam. This is valuable data for validations of sputter codes and the input parameters used for the codes, e.g. surface binding energies, displacement energies, and interaction potentials. Especially the surface binding energy has a crucial influence on sputtering, not only on the sputter yield. Commonly, the surface binding energy is estimated by the sublimation heat, typical values used in SRIM are: 1.35 eV for Zn, 2.97 eV for Ag, 3.52 eV for Cu, 4.34 eV for Fe, 4.46 eV for Ni, and 7.41 eV for C.[15] A slight change of these values can cause dramatic changes in the sputter yields. Comparisons between computer simulations and experiments are often done with respect to the sputter yield.[20–23] However, a bad model can still output a correct sputter yield when the surface binding energy is tuned appropriately. Since measurements with SPIN deliver a different integral quantity, which is not linearly related to the sputter yield, force measurements can either give enhanced confidence in a sputter code or reveal that unrealistic calculations are hidden behind a realistic sputter yield.

However, when the force exerted in the direction of the beam is to be measured, force probes like our previous one for the vertical beam setup,[9,10] or the one for a horizontal beam setup described in another paper of the proceedings at hand,[11] are to be chosen.

IV. Friction of microparticles and debris objects in a LEO

A microparticle or a heavier object in a low Earth orbit suffers friction due to collisions with air molecules of the rarefied atmosphere. This friction determines the residence time of the object in space.

A. Does sputtering play a role?

In order to calculate the friction force, one has to consider the impact events of the air molecules on the surface of the object. The speed of an object in a bound state (in general an elliptic orbit) cannot exceed the escape velocity $v_{\mathrm{esc}} \approx 11\,000\,\mathrm{m\,s^{-1}}$ in the inertial system of the Earth. For a circular orbit in a height of 200 km, its speed is $v = 7\,910\,\mathrm{m\,s^{-1}}$. The relative velocity between the object and an air molecule is only negligibly modified by the rotation of the Earth, wind, and thermal speed of the molecules. In case of an oxygen atom (most O_2 molecule are dissociated by ultraviolet radiation[14]), the upper speed limit v_{esc} corresponds to the kinetic energy of $E_{\mathrm{kin}} = 10\,\mathrm{eV}$ (18 eV for N_2, 10 eV for H_2O, and 26 eV for Ar).

These energies are clearly smaller than the sputter thresholds for most materials. For example, according to SRIM calculations, argon ions with $E_{\mathrm{kin}} = 32\,\mathrm{eV}$ impacting perpendicularly on a silver surface do not sputter at all, sputtering begins at approximately 33 eV and reaches a yield of 0.1 at 40 eV. In case of argon on copper, sputtering starts already at 27 eV, but this is still more than the kinetic energies of air molecules relative to an object bound to Earth.

Oxygen and nitrogen cannot be treated as diatomic molecules by SRIM, since the code applies the binary collision approach. The molecular binding energy is very small in comparison to the kinetic energies, so that the impacting molecules can be considered as two single atoms. However, the collision cascades are entangled and not independent of each other. This is not a problem in case of oxygen, which is mostly dissociated above 150 km according to the NRLMSISE-00 empirical atmospheric model.[14] To give an example, we consider atomic oxygen with the kinetic energy of $E_{\mathrm{kin}} = 10\,\mathrm{eV}$ impacting on a glass surface: according to the simulation, no sputtering is expected, and even 15 eV would not cause any sputtering.

B. Gas–surface interaction without sputtering

As we have shown in the previous subsection, sputtering by atmospheric molecules has no influence on the friction of a space debris object. However, in order to know the momentum transfer of an incident molecule to the surface of the object, an assumption on the kind of reflection has to be made. In case of specular reflection, i.e. the angle of incidence equals the angle of reflection, an incident atmospheric gas molecule would transfer *twice* the component of its momentum perpendicular to the surface to the latter. Such a model might be appropriate when the gas pressure on a wall is calculated where both the wall and the gas are in thermal equilibrium. Then the incident molecules keep their average energy when they are reflected,

and the velocity distribution function of the reflected particles equals the one for the incident particles when the sign of the velocity component perpendicular to the wall is inverted. In contrast, when the energy distribution of the incident particles does not equal the one of the temperature of the surface material, the average energy of the incident particles and their distribution function will change: an energetic beam would heat the target, and the released particles carry much less energy and momentum than before the impact. This effect is known as energy accommodation.

Even though the SRIM code was intended for the calculation of the interaction of ions with matter in the keV to MeV range, one could be curious and run SRIM for projectiles with the above mentioned kinetic energies. For example, 10 eV oxygen ions impacting perpendicularly on glass yield about 15 % backscattered oxygen ions (or atoms), and the remaining 85 % are stopped within 6 Å below the surface. Of course, the adsorbed oxygen would desorb later with much lower kinetic energy and momentum. The transferred momentum would be quite close to the momentum of the impinging particles. But this result should not be taken too seriously, which is shown in the following paragraph.

Tichmann et al. carried out molecular dynamics (MD) simulations for CH_3 molecules impinging at an angle of 38° on an amorphous hydrocarbon sample and compared them with results from SRIM.[24] Admittedly, this comparison is not fair in that it used SRIM to model a projectile that in reality consists of four atoms, because the code cannot treat the fragmenting of a projectile that happens at the impact. However, both simulations were in good agreement for kinetic energies above 50 eV, but showed completely different trends for low energies. While the sticking coefficients calculated by SRIM converged to 1 as E_{kin} approached 0, the MD value was about 0.5 for $E_{\mathrm{kin}} = 0$.

For an estimation of the drag force, we can conclude that the momentum transfer coefficients for the air molecules impacting on the object will be in the range $c_{\parallel} = (1 \ldots 2)$ for perpendicular incidence: A momentum transfer coefficient $c_{\parallel} = 1$ would result from adsorption of all the gas molecules and $c_{\parallel} = 2$ would require specular and elastic reflection. In case of arbitrary angles of incidence, the range is $c_{\parallel} = (0 \ldots 2)$, depending on the angle of incidence, the sticking coefficient, and the kind of reflection of the projectiles that do not stick. This extension of the possible values down to the limit $c_{\parallel} = 0$ is due to the molecules which are reflected to behind the object: these molecules transfer less than their initial momentum to the target. Obviously, a high sticking coefficient yields again a factor close to $c_{\parallel} = 1$.

Usually, instead of the momentum transfer coefficient, the drag coefficient c_{d} is used for orbit analysis. It is defined by the equation

$$F_{\mathrm{d}} = \frac{1}{2} c_{\mathrm{d}}\, v^2 \rho_{\mathrm{gas}}\, A_{\mathrm{eff}} \qquad , \tag{4}$$

which determines the drag force F_{d} at the speed v of the object relative to the gas molecules, when ρ_{gas} is the mass density of the atmosphere, and A_{eff} is the cross-sectional area of the moving object projected normally to the beam. For a plane target, $c_{\parallel}$ and $c_{\mathrm{d}}/2$ in Eq. (4) are obviously the same, since $v^2 \rho_{\mathrm{gas}}\, A_{\mathrm{eff}}$ describes the momentum influx due to the impinging gas molecules. However, the drag coefficient is usually used as a global parameter which describes the entire object.

Orbit analysts often use a drag coefficient of $c_{\mathrm{d}} = 2.2$ for compact satellites.[25] Today, several models and much data from orbital decay of satellites are available that allow a refined determination of the drag coefficient for a specific mission.[26] However, many parameters have an influence on the drag coefficient, where different models make use of their own selection of parameters. Such parameters besides material, speed, and angle of incidence, are the kind of reemission (diffuse, specular, quasi-specular, or other angular distributions), the energy accommodation, the coating of the surface by air molecules, e.g. physisorbed and chemisorbed oxygen, and the surface roughness.

If reliable accurate data for the drag coefficient is available, than the friction force exerted on the object can be calculated with higher precision. For example, in case of a spherical particle, the contributions from each surface element at the hemisphere exposed to the impacting molecules with its individual angle of attack have to be integrated to obtain the total friction force. This has been done for microparticles in an energetic ion beam ($E_{\mathrm{kin}} \leq 500\,\mathrm{eV}$), i.e. in the range where the SRIM code is valid.[17] In that situation, a momentum transfer coefficient of $c_{\parallel} = 1.05$ was obtained for a 400 eV beam, which corresponds to a drag coefficient of $c_{\mathrm{d}} = 2.1$. For the low energies of impacting air molecules in a LEO, e.g. 5.2 eV for oxygen, SRIM in its current version is unfortunately not the appropriate tool for generating the required data: nearly all of the atoms would apparently stick in the surface (even though released later diffusively with kinetic energies essentially accommodated to the target temperature), and the momentum transfer factor would be very close to $c_{\mathrm{d}} = 2$; actually c_{d} would even be slightly smaller, since some of the few backscattered atoms

(which occur predominantly at grazing incidence) are left behind the spherical particle and transfer less than their momentum to the particle. Realistic drag coefficients of spherical objects in low Earth orbits seem to have a range from $c_\mathrm{d} = 2.1 - 2.4$.[26]

V. Trajectories of model debris objects with atmospheric friction

In the following, we calculate exemplarily orbital lifetimes of spherical objects of different sizes starting in circular LEOs of different heights and assume the standard drag coefficient of $c_\mathrm{d} = 2.2$. The particles have the mass density of float glass $\rho_\mathrm{p} = 2230\,\mathrm{kg\ m^{-3}}$ and sizes (diameters) in the range from $1\,\mu$m to 10 mm. The particles start at heights from 150 km to 500 km at orbits with an inclination of 51.6 degrees to Earth's equator, which is, without any deeper meaning, the orbital inclination of the International Space Station (ISS).

The orbital lifetimes were calculated as follows. At first, the equation of motion for the particle at its starting height is integrated. The considered forces acting on the particle are gravity and the friction according to Eq. (4). The rotation of the atmosphere, wind, and thermal speeds are neglected. The density of the atmosphere at a given height is obtained from the NRLMSISE-00 empirical atmospheric model,[14] namely for the 172nd day of an undefined year. The lifetime of an object ends when its height drops below 80 km. If the lifetime exceeds one week, than a faster method is applied in order to avoid too long computation times and accumulated numerical integration errors. In such cases, the average friction at an orbit of a certain height is used to calculate the energy loss rate of the object $\dot{E} = \mathrm{d}E/\mathrm{d}t = F_\mathrm{d} v$, where v is the object's speed. The energy of the particle $E = E_\mathrm{kin} + E_\mathrm{pot}$ for a circular orbit is $E = -E_\mathrm{kin}$, where E_kin is the kinetic and E_pot is the potential energy. The algorithm takes the energy difference ΔE from the current orbit to a slightly lower orbit and calculates the transition time $\Delta t = \Delta E/\dot{E}$ to that orbit. The time integration is done by a two-step scheme, i.e. $\dot{E}$ is obtained from the friction F_d and the speed v at an intermediate orbit. When this coarse integration reaches a height at which the remaining orbital lifetime is already known and less than one week (one of the previously calculated cases), than this remaining orbital lifetime is used to complete the total lifetime.

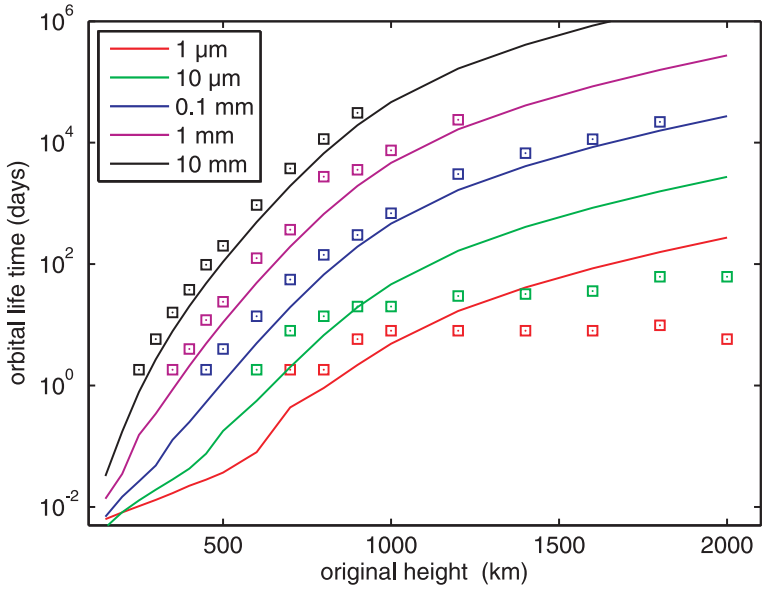

Figure 4. Calculated orbital lifetimes of spherical glass particles of different sizes on circular orbits (colored lines). For comparison, results from NASA's Debris Assessment Software are shown (correspondingly colored squares). The latter outputs only orbital lifetimes up to 100 years, and no times shorter than approximately nine hours could be retrieved.

The results are shown in Fig. 4. We compared the result with the Debris Assessment Software (DAS) from the NASA Orbital Debris Program Office.[27] This software uses also a drag coefficient of $c_\mathrm{d} = 2.2$, but a more sophisticated orbit propagator, which accounts also for solar and lunar gravity, solar radiation pressure, and higher harmonics of the Earth's gravity field. For the solar activity, regularly updated data is

used; the here presented calculations are for the date "2013.471", i.e. approximately June 21st, 2013, which was the 172nd day of this year. The markers in Fig. 4 show the results.

The orbital lifetime calculations by our own model and the DAS show reasonable agreement in case of the heavier objects ($\geq 0.1\,\mathrm{mm}$). The reason for the stronger discrepancies in case of the microparticles could be search for in the radiation pressure which affects more the smaller particles with bigger surface-to-mass ratios. The radiation pressure is accounted for only in the DAS model. A more detailed discussion of the results is beyond the scope of this proceedings paper, that focuses on the measurement of momentum transfer.

VI. Conclusion

This paper dealt some aspects of the momentum transfer at gas–surface interactions and its direct experimental determination by force probes. In space applications, such interactions occur in a variety of situations, e.g. inside of thrusters, at surfaces of instruments exposed to energetic particles that stem from thrusters, and at satellite or debris objects passing through the rarefied atmosphere in low Earth orbits. It was pointed out, that the physical mechanisms are different above and below the sputtering threshold energies. We presented the recently in our laboratory developed instrument SPIN for the measurement of sputtering related momentum transfer.[12,13] The special geometry makes the instrument insensitive for the momentum of the impinging beam particles themselves and measures only the momentum of the outgoing atoms. It was highlighted, that the instrument allows testing of sputter simulations beyond the comparison of sputter yields, since an agreement in the sputter yields is only a necessary, but not a sufficient criterion for the validity of a model. Beside SPIN, we made reference to another kind of force probe that measures the force component in the direction of incidence and is presented in a companion paper.[11]

The paper contains exemplary calculations of orbital lifetimes of debris objects. For simplicity, we assumed spherical glass particles as model debris. The results were compared to calculations with NASA's DAS software, which differs from our method in that it uses another atmospheric model for the calculation of the friction and includes solar radiation pressure for an additional acceleration term. However, the important drag coefficient of $c_\mathrm{d} = 2.2$ was the same in both calculations.

Unfortunately, drag coefficients are not well known. Force probes offer in principal an opportunity to measure directly the force exerted by the atmospheric gas on a surface. A force probe with sufficient precision aboard a satellite or the ISS could be equipped with targets of different materials and provide directly experimental data for drag coefficients. Such a force probe has to be able to measure pressures significantly below $10^{-8}\,\mathrm{N\ cm^{-2}}$. Furthermore, the angle of incidence of the gas molecules onto the target should be variable. We are currently working on a probe using an interferometric method, which should be able to fulfill such requirements.

Acknowledgments

This work was partly supported by the German Aerospace Center DLR, Projects No. 50 RS 0902 and No. 50 RS 1301.

References

[1]Kenmotsu, T., Wada, M., Hyakutake, T., Muramoto, T., and Nishida, M., "Erosion of accel grids of ion engine due to sputtering," *Rev. Sci. Instr.*, Vol. 81, 2010, pp. 02B109.

[2]Sengupta, A., Anderson, J. A., Garner, C., Brophy, J. R., De Groh, K., Banks, B., and Karniotis, T. A., "Deep Space 1 Flight Spare Ion Thruster 30,000-Hour Life Test," *J. Propul. Power*, Vol. 25, 2009, pp. 105–117.

[3]Yu, D., Li, Y., and Song, S., "Ion sputtering erosion of channel wall corners in Hall thrusters," *J. Phys. D: Appl. Phys.*, Vol. 39, 2006, pp. 2205–2211.

[4]Del Valle, J., Arce, N., Chinchilla, E., Echeverría, E., Lezama, D., Martínez, C., Oguilve-Araya, J., Rivera, A., Rodríguez, M., Valverde, J., Chang-Díaz, R., Olsen, C. S., Giambuso, M., Carter, M. D., Squire, J. P., and Chang-Díaz, F., "Measurement of the Dielectric Wall Erosion in Helicon Plasma Thrusters: an Application to the VASIMR VX-CR Experiment," *33rd International Electric Propulsion Conference, Washington, D.C., USA*, 2013, pp. IEPC–2013–188.

[5]Yalin, A., Topper, J., Farnell, C., Yoder, G., Hoang, B., and Corey, R., "Effect of Ion Sputtering on Transmission of Cover glass with Magnesium Fluoride Coating," *32nd International Electric Propulsion Conference, Wiesbaden, Germany*, 2011, pp. IEPC–2011–066.

[6]Bombardelli, C. and Peláez, J., "Ion Beam Shepherd for Contactless Space Debris Removal," *Journal of Guidance,*

Control, and Dynamics, Vol. 34, 2011, pp. 916–920.

[7]Brown, I. G., Lane, J. E., and Youngquist, R. C., "A lunar-based spacecraft propulsion concept – The ion beam sail," *Acta Astronautica*, Vol. 60, 2007, pp. 834–845.

[8]Ilin, A. V., Carter, M. D., Díaz, F. R. C., and Squire, J. P., "VASIMR Solar Powered Missions for NEA Retrieval and NEA Deflection," *33rd International Electric Propulsion Conference, Washington, D.C., USA*, 2013, pp. IEPC–2013–336.

[9]Spethmann, A., Trottenberg, T., and Kersten, H., "Measurement of the Momentum Flux in an Ion Beam," *32nd International Electric Propulsion Conference, Wiesbaden, Germany*, 2011, pp. IEPC–2011–232.

[10]Trottenberg, T., Spethmann, A., Schneider, V., Stahl, M., Giesenhagen, M., and Kersten, H., "Non-Electrostatic Diagnostics for Ion Beams," *Contrib. Plasma Phys.*, Vol. 52, 2012, pp. 584–592.

[11]Spethmann, A., Trottenberg, T., and Kersten, H., "Spatially Resolved Momentum Flux Measurements for Thruster Plume Diagnostics," *33rd International Electric Propulsion Conference, Washington, D.C., USA*, 2013, pp. IEPC–2013–079.

[12]Rutscher, J., Trottenberg, T., and Kersten, H., "An instrument for direct measurements of sputtering related momentum transfer to targets," *Nucl. Instr. and Meth. B*, Vol. 301, 2013, pp. 47–52.

[13]Trottenberg, T., Spethmann, A., Rutscher, J., and Kersten, H., "Non-electrostatic diagnostics for ion beams and sputter effects," *Plasma Phys. Control. Fusion*, Vol. 54, 2012, pp. 124005.

[14]Picone, J. M., Hedin, A. E., Drob, D. P., and Aikin, A. C., "NRLMSISE-00 empirical model of the atmosphere: Statistical comparisons and scientific issues," *J. Geophys. Res.*, Vol. 107, 2002, pp. 1468.

[15]Ziegler, J. F., Biersack, J. P., and Ziegler, M. D., *SRIM – The Stopping and Range of Ions in Matter*, SRIM Co., Chester, Maryland, 2008.

[16]Biersack, J. and Haggmark, L., "A Monte Carlo computer program for the transport of energetic ions in amorphous targets," *Nucl. Instr. and Meth.*, Vol. 174, 1980, pp. 257–269.

[17]Trottenberg, T., Schneider, V., and Kersten, H., "Measurement of the force on microparticles in a beam of energetic ions and neutral atoms," *Phys. Plasmas*, Vol. 17, 2010, pp. 103702.

[18]Phelps, A. V., "The application of scattering cross sections to ion flux models in discharge sheaths," *J. Appl. Phys.*, Vol. 76, 1994, pp. 747.

[19]Aberth, W. and Lorents, D. C., "Elastic Differential Scattering of He^+ Ions by Ne and Ar and of Ar^+ Ions by Ar in the 10–600-eV Range," *Phys. Rev.*, Vol. 144, 1966, pp. 109–115.

[20]Eckstein, W. and Biersack, J., "Sputtering investigations with the Monte Carlo program TRIM SP," *Nucl. Instr. and Meth. B*, Vol. 2, 1984, pp. 550–554.

[21]Wittmaack, K., "Reliability of a popular simulation code for predicting sputtering yields of solids and ranges of low-energy ions," *J. Appl. Phys.*, Vol. 96, 2004, pp. 2632–2637.

[22]Kotis, L., Menyhard, M., Toth, L., Zalar, A., and Panjan, P., "Determination of relative sputtering yield of Cr/Si," *Vacuum*, Vol. 82, 2007, pp. 178–181.

[23]Zalar, A., Kovač, J., Praček, B., Panjan, P., and Čeh, M., "Ion sputtering rates of W-, Ti-and Cr-carbides studied at different Ar^+ ion incidence angles," *Appl. Surf. Sci.*, Vol. 254, 2008, pp. 6611–6618.

[24]Tichmann, K., von Toussaint, U., Schwarz-Selinger, T., and Jacob, W., "Determination of the sticking probability of hydrocarbons on an amorphous hydrocarbon surface," *Phys. Scr.*, Vol. T138, 2009, pp. 014015.

[25]Cook, G. E., "Satellite drag coefficients," *Planet. Space Sci.*, Vol. 13, 1965, pp. 929–946.

[26]Moe, K. and Moe, M. M., "Gas–surface interactions and satellite drag coefficients," *Planet. Space Sci.*, Vol. 53, 2005, pp. 793–801.

[27]NASA Orbital Debris Program Office, "Debris Assessment Software (DAS), Version 2.0.2," 2013.